ANNIHILATION MOMENTUM DENSITY OF POSITRONS TRAPPED AT VACANCY-TYPE DEFECTS IN METALS AND ALLOYS*

A. Bansil
Physics Department
Northeastern University
Boston, MA 02115

R. Prasad
Department of Physics
Indian Institute of Technology
Kanpur, India 208016

R. Benedek
Materials Science Division
Argonne National Laboratory
Argonne, IL 60439

CONF-8706103--7

DE88 005936

January 1988

/pd

Paper to be published in Proc. Conf. on Alloy Phase Stability, NATO ASI, Chania, Crete, June 15-28, 1987.

*Work supported by the U.S. Department of Energy, BES-Materials Sciences, under Contracts DE-FG02-85ER45223 and #W-31-109-ENG-38.

ANNIHILATION MOMENTUM DENSITY OF POSITRONS TRAPPED AT VACANCY-TYPE DEFECTS IN METALS AND ALLOYS

A. Bansil

Physics Department, Northeastern University,
Boston, Massachusetts 02115

R. Prasad

Department of Physics, Indian Institute of Technology,
Kanpur, India 208016

R. Benedek

Materials Science Division, Argonne National Laboratory,
Argonne, Illinois 60439

I. INTRODUCTION

Positron annihilation, especially the angular correlation of annihilation radiation (ACAR), is a powerful tool for investigating the electronic spectra of ordered as well as defected materials. The tendency of positrons to trap at vacancy-type defects should enable this technique to provide a signature of the local environment of such defects. ~~an understanding of the changes in the defect structure at phase transitions is relevant also in the context of this conference.~~ In order to achieve this goal, however, we need to develop a theoretical basis for calculating the two-photon annihilation momentum density $\rho_{2\gamma}(\vec{p})$. With this motivation, we have recently formulated and implemented a theory of $\rho_{2\gamma}(\vec{p})$ from vacancy-type defects in metals and alloys.[1] This article gives an outline of our approach together with a few of our results. Within the constraints of space, the discussion is mostly illustrative; the citation of literature is minimal.

An outline of this article is as follows. Section II summarizes the basic equations for evaluating $\rho_{2\gamma}(\vec{p})$. Our Green's function-based approach is non-perturbative and employs a realistic (one-particle) muffin-tin Hamiltonian for treating electrons and positrons; we are therefore able to handle ordered as well as disordered d-band systems. Section III presents and discusses $\rho_{2\gamma}(\vec{p})$ results for a mono-vacancy in Cu.[1] These are the first such results in a d-band metal; previous work has been limited to Al.[2] For simplicity, we have neglected the effects of electron-positron correlations and of lattice distortion around the vacancy in our implementation of the theory; further work to delineate these effects is required. Section IV comments briefly on the question of treating defects such as divacancies and metal-impurity complexes in metals and alloys.[3] Finally, in Section V, we remark on the form of $\rho_{2\gamma}(\vec{p})$ for a mono-vacancy in jellium.[4]

II. FORMAL CONSIDERATIONS

The starting point for the Green's function formulation of $\rho_{2\gamma}(\vec{p})$ is the equation:

$$\rho_{2\gamma}(\vec{p}) = \frac{1}{\pi^2}\int d\vec{r}\int d\vec{r}'\, exp[-i\vec{p}\cdot(\vec{r}-\vec{r}')]\int dE\, f(E)\int dE_+\, f_+(E_+) \times Im\, G(\vec{r},\vec{r}';E)\; Im\, G_+(\vec{r},\vec{r}';E_+), \qquad (1)$$

which expresses $\rho_{2\gamma}(\vec{p})$ in terms of the electron and positron Green's functions $G(E)$ and $G_+(E)$, and the associated Fermi-Dirac distribution functions $f(E)$ and $f_+(E)$ respectively. In the present application, it is useful to rewrite Eq. (1) in the form

$$\rho_{2\gamma}(\vec{p}) = \sum_{mn} M_{mn}(\vec{p})\, e^{i\vec{p}\cdot(\vec{R}_m-\vec{R}_n)}. \qquad (2)$$

Equation (2) decomposes $\rho_{2\gamma}(\vec{p})$ into a summation over the set $\{\vec{R}_m\}$ of direct lattice vectors with matrix elements $M_{mn}(\vec{p})$.

A computationally tractable equation for the matrix elements $M_{mn}(\vec{p})$ is obtained by using the angular momentum expansion for the Greens' function within the KKR scheme:[5]

$$Im\, G(\vec{r}_1,\vec{r}_2,E) = \sum_{LL'} Z_L^{(m)}(\vec{r}_1-\vec{R}_m,E)\; Im\, T_{LL'}^{mn}\; Z_{L'}^{(n)}(\vec{r}_2-\vec{R}_n,E), \qquad (3)$$

where $\vec{r}_1(\vec{r}_2)$ lies in the Wigner Seitz cell on the $m(n)$ site, $Z_L^{(i)}$ is the regular solution of the Schrödinger equation in the i^{th} muffin-tin sphere, and

$$T(E) = [\tau^{-1} - B(E)]^{-1}, \qquad (4)$$

is the path operator matrix in the space of site indices n and the angular momenta L. B is similarly a matrix which in a perfect crystal is the Fourier transform of the KKR structure constants, and the atomic scattering matrix τ is related to the phase shifts of the individual scatterers. The use of expansion (3) for the electron and the positron Green's function straightforwardly yields the expression:

$$M_{mn}^{\alpha\beta}(\vec{p}) = \frac{1}{\pi^2}\int dE f(E)\int dE_+ f(E_+)\sum_{L_1L_1'}\sum_{L_2L_2'}\Delta_{L_1L_2}^{m\alpha}(\vec{p},E,E_+) \times \Delta_{L_1'L_2'}^{n\beta}(-\vec{p},E,E_+)[Im\, T_{L_1L_1'}(E)\, Im\, T_{L_2L_2'}(E_+)], \qquad (5)$$

where

$$\Delta_{LL'}^{i\alpha}(\vec{p},E,E_+) = 4\pi\sum_{L''}(-i)^{l''}Y_{L''}(\hat{p})\int_{\Omega_i} d^3r\; Z_L^{e,i\alpha}(\vec{r},E)\, Z_{L'}^{p,i\alpha}(\vec{r},E_+)Y_{L''}(\hat{r})\, j_{l''}(pr). \qquad (6)$$

The superscript $\alpha(\beta)$ in Eqs. (5) and (6) indicates that the site m(n) is occupied by atom of type $\alpha(\beta)$; the superscript e(p) refers to electron(positron) quantities. The integration in Eq. (6) extends over the i^{th} cell volume Ω_i.

The preceding formalism can, in principle, be used to calculate $\rho_{2\gamma}(\vec{p})$ for a general assembly of non-overlapping muffin-tin scatterers; we return to the treatment of specific defects below. It should be emphasized that the present real space approach is particularly suitable for evaluating $\rho_{2\gamma}(\vec{p})$ from a trapped positron, because the exponential decay of the positron wave-function from the trapping site will yield a rapid convergence of the sum in Eq. (2); by contrast, $\rho_{2\gamma}(\vec{p})$ for an extended Bloch-state positron is more naturally calculated by formally transforming these summations into reciprocal space.

III. MONO-VACANCY IN Cu

In any specific case, the main quantities which require further consideration are the electron and positron path operators T^e and T^p. For a mono-vacancy in an otherwise perfect crystal, the path operators can be obtained by using the exact solutions of the multiple scattering equations for the single impurity problem,[5] the impurity in the present case being the vacant site. For example, the (00) electron path operator is given by the equation:

$$T_v^{e,00}(E) = D_v(E)\, T^{e,c,00}(E), \tag{7}$$

where $T^{e,c,00}$ is the perfect crystal path operator, and

$$D_v(E) = [1 + (\tau_v^{-1}(E) - \tau_c^{-1}(E))\, T^{e,c,00}(E)]^{-1}. \tag{8}$$

Here, τ_v and τ_c refer to the electron muffin-tin potential for the vacant and the occupied crystalline sites respectively.

We have studied $\rho_{2\gamma}(\vec{p})$, and related physical quntities such as the electron and positron charge densities for a mono-vacancy trapped positron in Cu in some detail. Figure 1 shows illustrative results for $\rho_{2\gamma}(\vec{p})$. More specifically, partially summed contributions $\rho_{2\gamma}^{(j)}(\vec{p})$ upto the 4th shell are shown; the superscript (j) indicates the number of the most distant shell (surrounding the vacant site) upto which contributions to $\rho_{2\gamma}(\vec{p})$ in Eq. (2) are included. A comparison of the $j = 1$ through $j = 4$ curves (the $j = 3$ and $j = 4$ curves are indistinguishable on the scale of the figure) indicates that $\rho_{2\gamma}^{(1)}(\vec{p})$ is converged to within 10% of $\rho_{2\gamma}(\vec{p})$. We note that, $\rho_{2\gamma}^{(1)}(\vec{p})$ possesses all the characteristic features of the fully converged momentum density curve.

Figure 1 shows that the $j = 0$ (vacancy site) contribution to $\rho_{2\gamma}(\vec{p})$ is quite flat and featureless. The addition of the nearest neighbor (110)-shell(nn) contribution (the $j = 1$ curve) causes a dramatic change in $\rho_{2\gamma}(\vec{p})$ in the low momentum region. In fact, for $p \leq 5$ mrad, $\rho_{2\gamma}(\vec{p})$ is dominated by the nn-shell contribution. This may appear surprising in view of the exponential decay of the trapped positron wave function from the vacant site. We note however that $\rho_{2\gamma}(\vec{p})$ involves an overlap of the electron and positron wave functions. In the vacant site, the positron amplitude is large, but the electron density is quite small; on the other hand, in the nn-sites, a large electron density annihilates with the tail of the positron wave function. Therefore, the central site and nn-shell contributions should both be generally important. The exponential

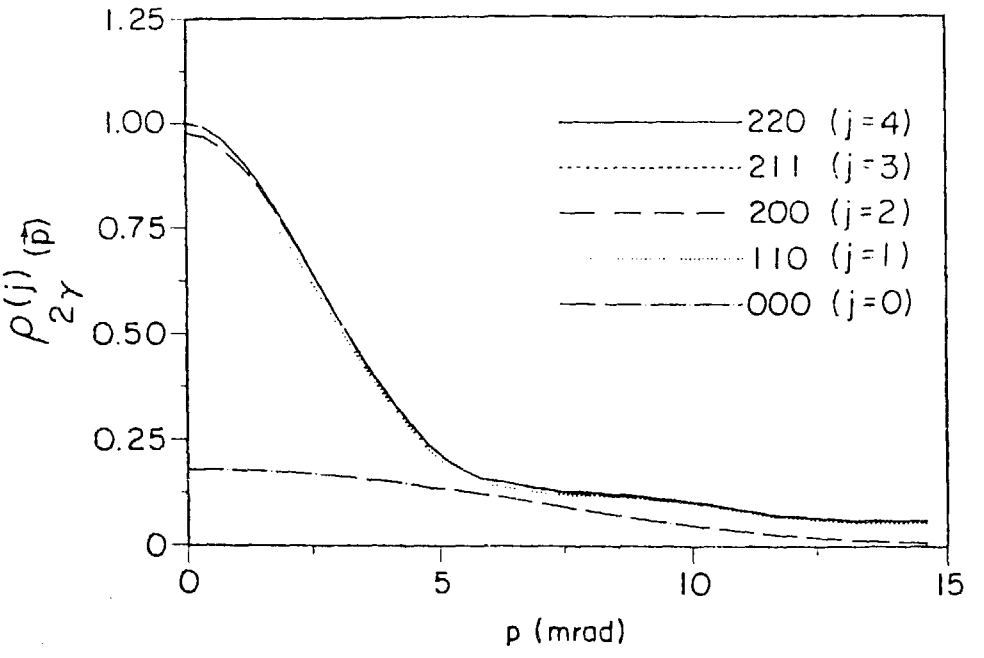

FIGURE 1: Partially summed momentum density $\rho_{2\gamma}^{(j)}(\vec{p})$ along [001] direction for various shells j for a mono-vacancy in Cu. After Ref. [1].

decay of the positron wave function makes contribution from more distant shells much smaller. Our calculations suggest that the nn-shell contributions would dominate in the low-p region more generally for mono-vacancies in metals and alloys.

IV. TREATMENT OF OTHER VACANCY-TYPE DEFECTS

We have in mind here situations which can be modelled by considering a relatively small (i. e. involving at most a few shells surrounding a central site) "defected region" placed in an otherwise perfect ordered medium. We consider a divacancy in Cu to illustrate our approach. If the system is modelled by placing two vacant sites in a perfect Cu crystal, we need to solve the "two impurity" path operator. By using matrix partitioning methods, the problem can be cast in terms of a (2×2) matrix equation (in angular momentum space) involving perfect Cu crystal path operators; the latter path operators are needed of course also for treating the mono-vacancy in Cu. The generalization to an impurity cluster of M-sites is quite straightforward, the solution is obtained then via an $(M \times M)$ matrix equation; see Ref. [3] for details of evaluating $\rho_{2\gamma}(\vec{p})$.

We comment finally on the treatment of vacancy type defects in disordered alloys. Here we need to ensemble average both sides of Eq. (2); this step formally yields:

$$< \rho_{2\gamma}(\vec{p}) >= \sum_{mn} < M_{mn}(\vec{p}) > e^{i\vec{p}\cdot(\vec{R}_m - \vec{R}_n)}, \qquad (9)$$

where $< M >$ is seen from Eq. (5) to require the configuration average of the product $< Im\,T^e\ Im\,T^p >$ of electron and positron path operators; in Ref. [1] we propose to

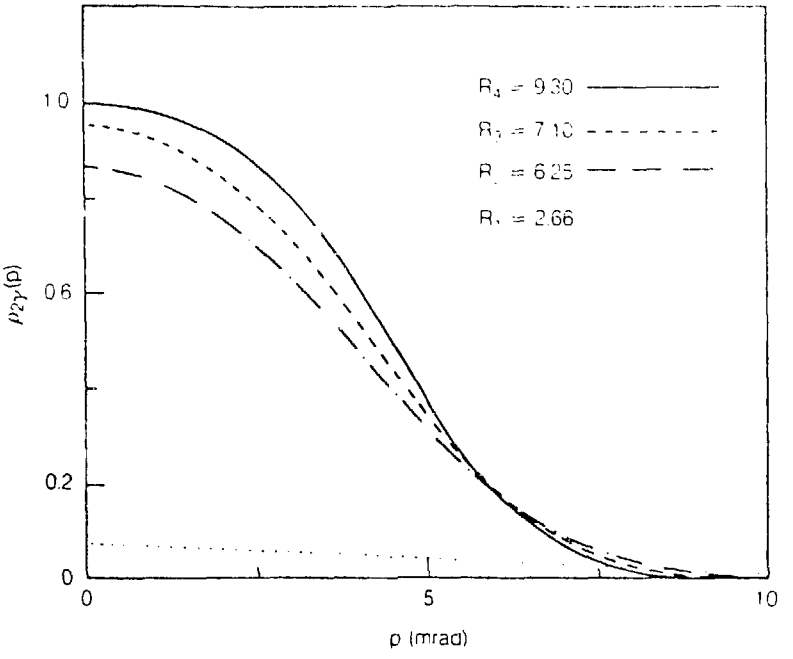

FIGURE 2: $\rho_{2\gamma}(\vec{p})$ for a mono-vacancy in jellium for various values of the radius R of the integration volume(see text). After Ref. [4].

decouple this average in terms of the electron and positron KKR-CPA medium path operators. Tractable expressions for $< \rho_{2\gamma}(\vec{p}) >$ are than straightforwardly obtained; see Ref. [1] for details.

V. MONO-VACANCY IN JELLIUM

A mono-vacancy in jellium is interesting because this model is amenable to an exact analytic solution at least for certain idealized potentials. We have used this model system to gain insights into the results obtained on the basis of the Green's function-based approach. Figure 2 shows $\rho_{2\gamma}(\vec{p})$ for a vacancy in jellium using a square well (square barrier) potential for positron (electrons).[4] The various parameters (well depth, barrier height, and Fermi energy) are chosen to mimic a mono-vacancy in Cu. The parameter R in the figure denotes the radius of the spherical volume to which the electron-positron overlap integral is restricted in calculating $\rho_{2\gamma}(\vec{p})$ (i.e. restrict $|\vec{r}|, |\vec{r}'| \leq R$ in the integrations in Eq. (1)); the values R_j correspond to an integration sphere of volume enclosed by the first j shells in Cu. Some of the characteristic features of Fig. 1 are seen to be reproduced by the model system. In particular, the magnitude of the R_1 curve is relatively small as is the case with the central site contribution in Fig. 1. Also, the R_2 curve shows the striking bell-shape of the $\rho_{2\gamma}^{(1)}(\vec{p})$ curve of Fig. 1; in contrast, as is well-known, $\rho_{2\gamma}(\vec{p})$ for the Bloch-state positron in Cu possesses an approximately constant value of unity up to the Fermi energy. It is clear that the jellium model can be useful in understanding the behavior of $\rho_{2\gamma}(\vec{p})$, although the model does not properly incorporate the Fermi surface and the d-bands in the electronic spectrum, in addition to neglecting the effects of nuclear

repulsion of the positron from the host metal sites.

One of us (R.P.) acknowledges the hospitality of the Physics Department, Northeastern University, where part of this work was completed. This project was supported by the U. S. Department of Energy, BES-Materials Science, under contracts DE-FG02-85ER45223 and W-31-109-Eng- 38. It benefited from an allocation of supercomputer time on the ER-Cray at the MFE computer center.

REFERENCES

1. R. Prasad, R. Benedek, and A. Bansil in **Positron Annihilation**, edited by P. C. Jain, R. M. Singru, and K. P. Gopinathan (World Scientific, Singapore, 1985), p. 859; R. Prasad, R. Benedek, J. E. Robinson, and A. Bansil (to be published).
2. R.P. Gupta and R.W. Siegel, Phys. Rev. Letters **39**, 1212(1977); Phys. Rev. **B22**, 4572(1980); B.Chakraborty and R.W.Siegel, Phys. Rev.**B27**,4535(1983).
3. R. Prasad, A. Bansil, and R. Benedek (to be published).
4. J.E. Robinson, R. Benedek and R. Prasad, Phys. Rev. **B35**, 7392(1987).
5. For a recent review of the Green's function treatment of the electronic structure of ordered and disordered systems, see A. Bansil, in **Electronic Band Structure and its Applications**, Lecture Note Series, Vol. 283 (Springer-Verlag, Heidelberg, 1987), p. 273.